RSC Advances

PAPER

View Article Online
View Journal | View Issue

Cite this: *RSC Adv.*, 2021, **11**, 33431

One-pot synthesis of conjugated triphenylamine macrocycles and their complexation with fullerenes†

Ying-Bo Lu,[a] Shinji Kanehashi,[a] Kazushi Minegishi,[a] Shu-Ping Wang,[b] Jin Cheng,[a] Kenji Ogino*[a] and Shijun Li *[b]

Received 16th August 2021
Accepted 4th October 2021

DOI: 10.1039/d1ra06200j

rsc.li/rsc-advances

Triphenylamine derivates have been utilized as building blocks in hole-transporting materials. Herein, we describe the synthesis of three octyl-derived conjugated triphenylamine macrocycles with different sizes, and a 4-(2-ethylhexyloxy)-substituted cyclic triphenylamine hexamer using a palladium-catalyzed C–N coupling reaction. These conjugated triphenylamine macrocycles not only have interesting structures, but also are capable of complexing with C_{60}, C_{70} and $PC_{61}BM$. Their binding stoichiometries with fullerenes were all determined to be 1 : 1 by an emission titration method. The association constants of these complexes were measured to be in the range of 0.115–1.53 $\times$ 10^5 M^{-1} depending on the cavity size of the triphenylamine macrocycles and the volume of the fullerenes. The space-charge-limited current properties of the complexes were further investigated using the fabricated ITO/PEDOT:PSS/active layer/Au devices.

Introduction

Triphenylamine (TPA) is a strong electron donor that has been widely used in various organic optoelectronic devices.[1–3] Materials based on TPA show extremely good hole-transporting performance and high stability, even though they have a high hole-injection barrier and low mobility. Among them, TPA oligomers have attracted much attention in recent years because they showed the complementary advantages of both polymers and low molecular weight organic compounds, such as high thermal stability and possibility in purification. The TPA oligomer with a spiro structure is one of the most outstanding examples, which has been widely studied because of its unique rigid spiro structure.[4–8]

Conjugated cyclic oligomers usually have a highly symmetrical architecture, and play a significant role in optoelectronic science.[9–18] Oligomers possessing cyclic structures are different from other oligomers due to the absence of terminal groups, which gives cyclic oligomers a very uniform electron distribution. The cyclic structures also offer the opportunity for better thermal stability and higher packing capability in solid state. Furthermore, as a class of macrocycles with large molecular cavities, the conjugated cyclic oligomers are qualified to incorporate other guest molecules with appropriate sizes. These features endow the conjugated cyclic oligomers great potential applications in a wide range of fields, such as chemical sensors, molecular switches, light-harvesting antennae, and organic light-emitting diodes.[19–23]

Fullerenes are well-known as a class of electron acceptors and are one of the most used guest molecules since it was reported by Curl, Kroto and Smalley in 1985.[24] Owing to their unique photophysical properties,[25,26] fullerenes and their derivatives have been extensively applied in pharmaceuticals,[27–29] electronic and photovoltaic materials.[30–33] Moreover, fullerenes could complex with conjugated macrocycles consisting of phenylene,[34] thiophene,[35–37] or other heterocyclic rings,[38–41] which have significant application prospect in organic optoelectronics. Although there had a few examples involving the complexation between TPA compounds and fullerenes,[42,43] the research on conjugated cyclic triphenylamine (CTPA) complexed with fullerenes has not been reported so far.

Our group reported a method to synthesis triphenylamine-containing conjugated macrocycles with three different sizes in 2011.[44] It was demonstrated that the cyclic pentamer CBTPA [5] exhibited high thermal stability and a hole mobility of nearly 100 times as compared with the corresponding linear polymer.[45] The CTPAs are significantly better than the linear TPA in various optoelectronic properties, but synthesis of CTPAs by the previous method needs tedious separation of three macrocycles with different sizes, but similar polarity.

[a]*Graduate School of Bio-Applications and Systems Engineering, Tokyo University of Agriculture and Technology, 2-24-16 Nakacho, Koganei, Tokyo, 184-8588, Japan. E-mail: kogino@cc.tuat.ac.jp*

[b]*College of Material, Chemistry and Chemical Engineering, Hangzhou Normal University, Hangzhou, 311121, P. R. China. E-mail: l_shijun@hznu.edu.cn*

† Electronic supplementary information (ESI) available: Characterization data of the CTPAs and investigation data on complexation of CTPAs with fullerenes. See DOI: 10.1039/d1ra06200j

Herein, we developed a new method for selective preparation of the cyclic TPA hexamer and comparatively synthesized three solubility-improved CTPAs using our previous method. The structures and sizes of these CTPAs was evaluated and compared by employing density functional theory (DFT), and the complexation between these synthesized CTPAs and fullerenes were investigated.

Results and discussion

Three octyl-derived cyclic TPA oligomers with different sizes, named **COTPA [5]**, **COTPA [6]** and **COTPA [7]**, were firstly synthesized through one-pot C–N coupling method.[44] Polymeric byproducts were removed by a convenient Soxhlet extraction based on the insolubility of polymers in butanone. The linear and cyclic oligomers were separated each other by a silica gel column chromatography since the former possesses polar secondary amino group, and the latter not. As shown in Table S1,† **COTPAs** [5], [6], and [7] showed different solubilities, but not enough to isolate each oligomer by a crystallization process. Since molecular polarities of cyclic oligomers are quite similar, it was necessary to utilize a preparative gel permeation chromatographic method for the isolation of **COTPAs**. To further polish this time-consuming synthetic method, a new alternative strategy to selectively prepare a cyclic TPA hexamer **CETPA [6]** was developed, by which tedious separation process of CTPAs could be avoided (Scheme 1). In this new method, 4,4′-dibromo-1,1′-biphenyl was used as a starting compound, which was reacted with excessive *para*-substituted aniline to prepare the di-substituted monomer **2**. Unlike monomer **1**, there are two reactive sites where C–N coupling could carry out on the monomer **2**. Therefore, TPA units in the product would be an even number when monomer **2** couples with 4,4′-dibromo-1,1′-biphenyl in a cyclic modality. Owing to the ~120° bond angle of TPA, C–N coupling cyclization of **2** seemed very difficult to form a cyclic tetramer or octamer.[44] As a desired result, the reaction delivered the cyclic TPA hexamer as a sole cyclic product. No any other cyclic oligomers were observed. Structure of the prepared cyclic hexamer **CETPA [6]** was confirmed by ^{1}H NMR, ^{13}C NMR and MALDI-TOF-MS (Fig. S15–S17†) (Scheme 2).

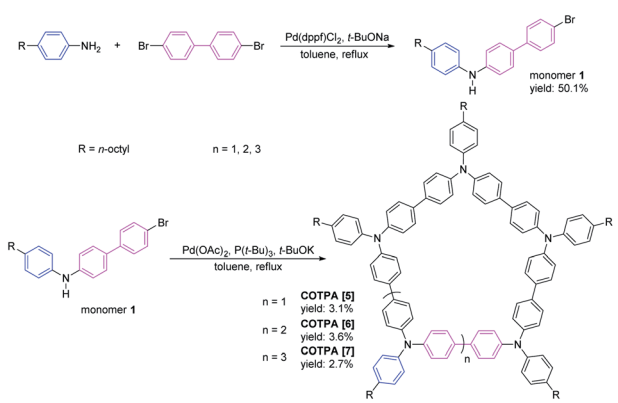

Scheme 1 Synthesis of **COTPA [5]**, **COTPA [6]** and **COTPA [7]**.

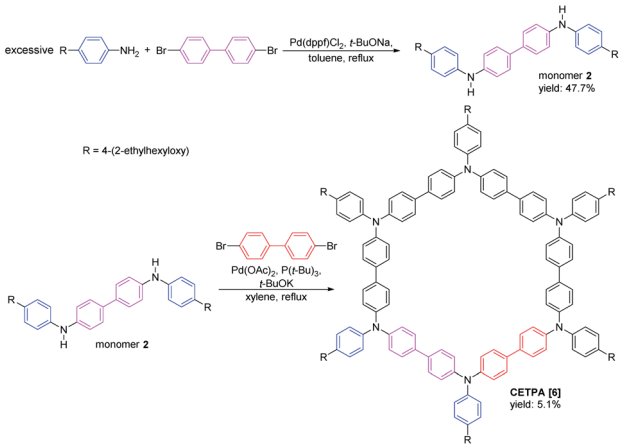

Scheme 2 Synthesis of **CETPA [6]**.

Host–guest complexation of the synthesized CTPAs with fullerenes was then investigated by UV-vis absorption spectroscopy and fluorescence spectroscopy (Fig. 1). As a result of π–π stacking and donor–acceptor interactions between **COTPA [7]** and fullerenes, a slight red shift in absorption spectroscopy was observed accompanied by an obvious absorption decrease (Fig. 1a). The red shift of C_{70}⊂**COTPA [7]** (from 347 nm to 351 nm) is more distinct than that of C_{60}⊂**COTPA [7]** and PC_{61}BM⊂**COTPA [7]**, which is probably due to that both the short (0.712 nm) and long (0.796 nm) axis of C_{70} (ref. 46) are longer than the molecular diameter of C_{60} (0.710 nm), and the larger

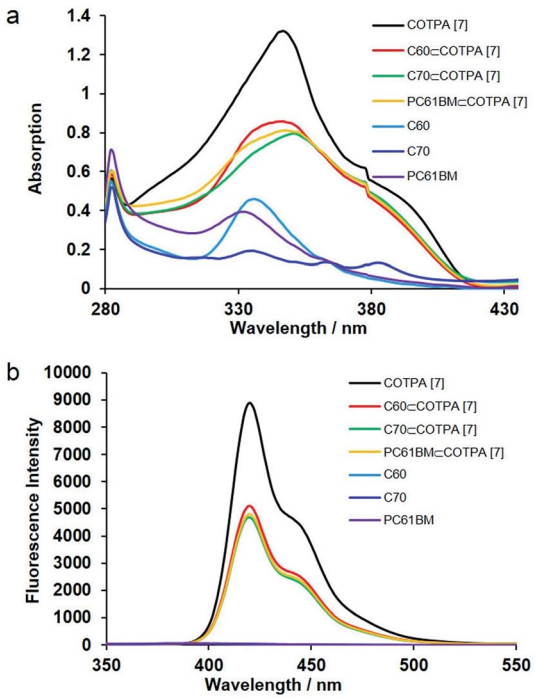

Fig. 1 (a) UV-vis and (b) fluorescence (λ_{ex} = 300 nm in toluene, 5 × 10^{-6} M, 298 K) spectra of **COTPA [7]**, C_{60}⊂**COTPA [7]**, C_{70}⊂**COTPA [7]**, PC_{61}BM⊂**COTPA [7]**, C_{60}, C_{70} and PC_{61}BM.

Table 1 K_a (M^{-1}) calculated by modified Benesi–Hildebrand equation using fluorescence spectroscopy (λ_{ex} = 300 nm in toluene, 5×10^{-6} M, 298 K)

	C_{60}	$PC_{61}BM$	C_{70}
COTPA [5]	$(1.15 \pm 0.08) \times 10^4$	$(8.42 \pm 0.60) \times 10^4$	$(1.07 \pm 0.79) \times 10^5$
COTPA [6]	$(1.53 \pm 0.07) \times 10^4$	$(9.00 \pm 0.59) \times 10^4$	$(1.01 \pm 0.05) \times 10^5$
COTPA [7]	$(2.71 \pm 0.11) \times 10^4$	$(1.53 \pm 0.16) \times 10^5$	$(1.05 \pm 0.07) \times 10^5$
CETPA [6]	$(2.26 \pm 0.18) \times 10^4$	$(8.41 \pm 0.47) \times 10^4$	$(9.79 \pm 0.48) \times 10^4$

contact area leads to the stronger red shift of C_{70}⊂**COTPA [7]**. Fig. 1b showed that the emission of **COTPA [7]** in toluene appeared at λ = 420 nm when it was exited at λ = 300 nm and the addition of fullerene decreased the intensity of emission at λ = 420 nm. Similar phenomenon was also observed in the absorption and emission spectroscopy of fullerenes⊂**COTPA [5]** and fullerenes⊂**CTPAs [6]** (Fig. S18–S21†). These all supported the presence of strong complexation between CTPAs and fullerenes.

The binding stoichiometries for all of the complexes C_{60}⊂CTPAs, C_{70}⊂CTPAs, $PC_{61}BM$⊂CTPAs were determined to be 1 : 1 by using the mole ratio method (Fig. S22–S33†). The binding constants (K_a) of C_{60}⊂**COTPA [5]**, C_{60}⊂**COTPA [6]**, C_{60}⊂**CETPA [6]** in toluene were estimated to be $(1.15 \pm 0.08) \times 10^4$ M^{-1}, $(1.53 \pm 0.07) \times 10^4$ M^{-1} and $(2.26 \pm 0.18) \times 10^4$ M^{-1}, respectively, while K_a of C_{60}⊂**COTPA [7]** in toluene was measured to be $(2.71 \pm 0.11) \times 10^4$ M^{-1} (Table 1 and Fig. S34–S45†). It was demonstrated that the K_a value was slightly influenced by the side chain and ring size of CTPAs. When the size of CTPAs increases from pentamer to hexamer, K_a enhances slightly. The heptamer has a higher K_a than those of pentamer and hexamer, the main reason of which is probably the cavity size of heptamer being more suitable to incorporate C_{60}. As a result, the volume of C_{60} that sunk into cyclic heptamer is larger than that of pentamer and hexamer. A similar trend was found for $PC_{61}BM$⊂CTPAs. As a matter of fact, there were a few reports demonstrated the cavity size of cyclic oligomers had notable influence on the binding pattern and K_a of host–guest complexes.[34,47] Nonetheless, when the fullerene C_{70} with an increased size was used as guest, almost no difference was found in K_a of these complexes, which is most probably due to that the oversized guest C_{70} does not deeply sink into the cavity of CTPAs, but laterally approaches CTPAs with almost the same contact area. On the other hand, as we compare association constants of the same CTPA, the K_a of C_{70}⊂CTPAs are generally higher than those of C_{60}⊂CTPAs and $PC_{61}BM$⊂CTPAs (except $PC_{61}BM$⊂**COTPA [7]**). This result could also be attributing to the larger contact area of C_{70}, which is in agreement with the trend observed in the absorption spectra (Fig. 1a). Meanwhile, the K_a of $PC_{61}BM$⊂CTPAs are universally higher than those of C_{60}⊂CTPAs, reasonably owing to the side chains of $PC_{61}BM$ that furnish extra supramolecular interactions with the alkyl chains on the CTPAs.

To evidence our conjecture, the DFT calculations were employed to investigate the geometry structures of **COTPA [5]**, **COTPA [6]** and **COTPA [7]** by using a Gaussian program (Fig. 2).[48] The internal cavity diameter of **COTPA [5]** in the optimized structure is estimated about 1.05–1.16 nm, which is considered difficult to be threaded by C_{60}. The cavity diameter of **COTPA [6]** and **COTPA [7]** are around 1.34–1.41 nm and 1.56–1.65 nm, similar or slightly higher than the requisite size that macrocycles could incorporate C_{60}, as evaluated in the previous reports.[9,11] By comparing the side view of **COTPA [6]** and **COTPA [7]**, we found the side chain of **COTPA [7]** was not as planar as **COTPA [6]** owing to the twisted cyclic structure of **COTPA [7]** (Fig. S46†). This might enhance the binding capability of **COTPA [7]** and thus increase the stability of fullerene⊂**COTPA [7]**.

Finally, **COTPA [5]** or its complex with C_{60} was preliminarily applied to a diode device, which is a basis for

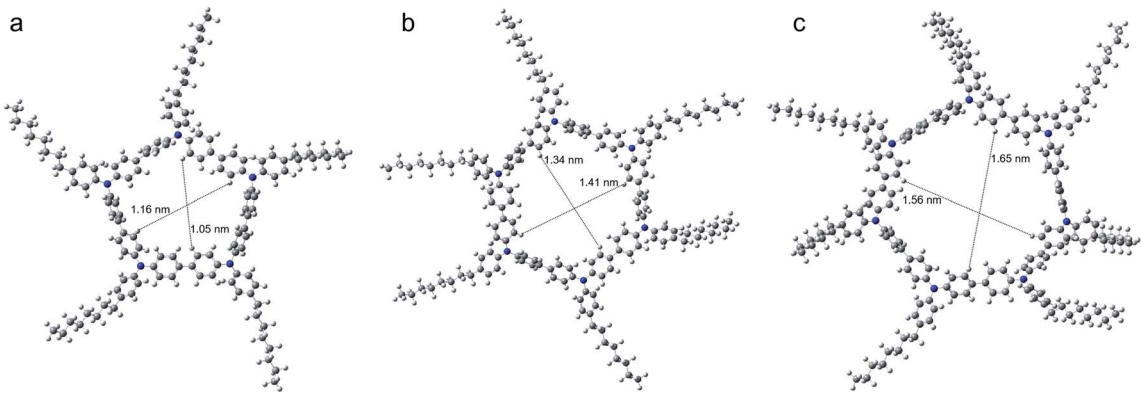

Fig. 2 Top view of DFT optimized structure of (a) **COTPA [5]**, (b) **COTPA [6]**, (c) **COTPA [7]** and the estimated internal diameters of them.

electroluminescent and photovoltaics devices. The space-charge-limited current (SCLC) mobility was estimated while the device with the configuration of ITO/PEDOT:PSS/**COTPA [5]** or **COTPA [5]** blended with C_{60}/Au exhibits the SCLC behavior (Fig. 3). The SCLC mobilities were calculated using the following equation:

$$J = (9/8)\varepsilon_r\varepsilon_0\mu(V^2/L^3)$$

where ε_r is the dielectric constant ($\varepsilon_r = 2.3$), ε_0 is the permittivity of free space, L is the thickness of the active layer, μ is the mobility of active layer, and V is the applied voltage. It was found that the calculated average mobility of **COTPA [5]** blended with C_{60} (1.56×10^{-4} cm^2 V^{-1} s^{-1}, estimated from 3 devices) was 8 times higher than that of **COTPA [5]** (1.91×10^{-5} cm^2 V^{-1} s^{-1}, estimated from 6 devices), indicative of that the addition of C_{60} could enhance the hole mobility, probably due to the establishment of transporting path resulting from the complexation.

Further investigation on the self-assembly behavior of **COTPA [5]** and $C_{60}\subset$**COTPA [5]** was carried out by TEM (transmission electron microscope) observation. The **COTPA [5]** solution in toluene (1×10^{-3} mol L^{-1}) was casted on a copper mesh grid. As shown in Fig. 4a and b, **COTPA [5]** self-assembled into irregular-shaped aggregates. Whereas a mixture solution of **COTPA [5]** and C_{60}, both of them at 1×10^{-3} mol L^{-1}, afforded entirely different morphology as shown in Fig. 4c and d. At lower magnification (c), it is found that a number of fibers with length of a micron range are bundled around at the center. In the expanded image (d), we can observe that each fiber consists of the aggregation of finer fibric structures. This striking morphology probably resulted from the alternate connection of **COTPA [5]** and C_{60} due to the sandwich-like complexation, which may cause the improvement of electron conductivities of these materials.

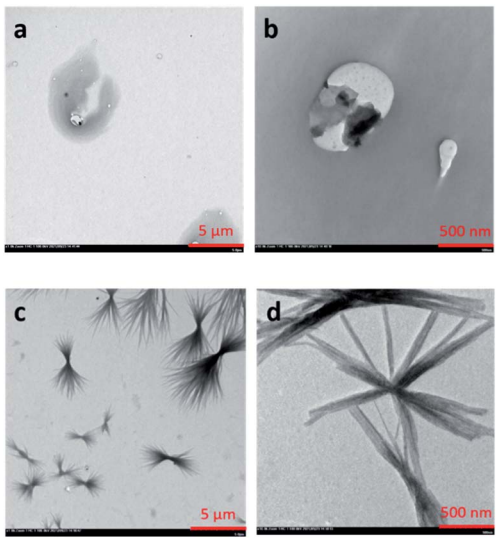

Fig. 4 TEM images of **COTPA [5]** (a, b) and **COTPA [5]** blend with C_{60} (c, d).

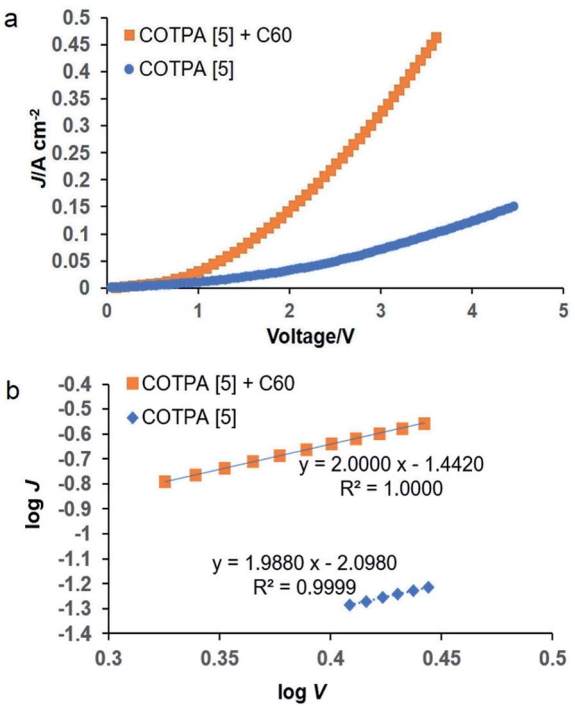

Fig. 3 (a) Current density–voltage (J–V) curves and (b) SCLC curves of the ITO/PEDOT:PSS/**COTPA [5]** or **COTPA [5]** blend with C_{60}/Au device.

Conclusions

We have synthesized conjugated cyclic pentamer, hexamer and heptamer consisting of TPA, and develop a new method to synthesis cyclic TPA hexamer. These CTPAs could complex with C_{60}, $PC_{61}BM$ and C_{70} in 1 : 1 binding stoichiometries. The association capability of CTPAs toward C_{60} or $PC_{61}BM$ depends on the macrocycle sizes of CTPAs, while the sizes of CTPAs have no apparent influence on their complexation with C_{70}. **COTPA [5]** and its complex with C_{60} were further applied in optoelectronic devices. The average hole mobility of **COTPA [5]** blended with C_{60} was found to be 1.56×10^{-4} cm^2 V^{-1} s^{-1}, 8 times higher than that of **COTPA [5]**.

Experimental

Materials and methods

Unless otherwise stated, chemicals and solvents were used as purchased from commercial sources and without further purification. 4-Octylaniline, sodium *t*-butoxide, and potassium *t*-butoxide were received from Tokyo Chemical Industry. 4-Nitrophenol, 3-(bromomethyl)heptane, potassium carbonate, palladium carbon, palladium acetate, *tri*(*t*-butyl)phosphine, methanol, hexane, *c*-hexane, 4,4′-dibromobiphenyl, dichloro [1,1′-bis(diphenylphosphino)ferrocene]palladium(II), magnesium sulphate, super-dehydrated toluene, super-dehydrated xylene, *o*-xylene, *N*,*N*-dimethylformamide, and ethanol, were received from Fujifilm Wako Chemicals. NMR spectra were

recorded on a Bruker ADVANCE III 500 MHz spectrometer or a JEOL JNM-ECX300 (300 MHz) spectrometer at room temperature. ^{1}H NMR and ^{13}C{^{1}H} NMR chemical shifts (δ) are given in ppm and are reported relative to tetramethylsilane (TMS) at 0.00 ppm or the residual solvent signals. Mass spectra were recorded on a Bruker autoflex III smartbeam MALDI-TOF spectrometer. UV-vis spectra were recorded on a PerkinElmer Lambda 750 visible spectrophotometer. Emission spectra were recorded on a Hitachi F-7000 at room temperature. Transmission electron microscope (TEM) was performed at 120 kV using JEM-2010. The TEM samples were prepared as following: The solutions of CTPAs or equimolar mixture of CTPAs and fullerenes were cast on carbon-coated grids (Cu, 400 mesh) and dried naturally at room temperature before TEM photography.

Synthesis of monomer 1

4-Octylaniline (20.10 g, 97.96 mmol), 4,4′-dibromobiphenyl (30.36 g, 97.96 mmol), sodium *t*-butoxide (9.41 g, 97.96 mmol), dichloro[1,1′-bis(diphenylphosphino)ferrocene]palladium(II) (797.4 mg, 0.92 mmol) and super-dehydrated toluene (100 mL) was added in a 250 mL flask under nitrogen atmosphere. The reactant was stirred and refluxed for 12 h. After completion of the reaction, the mixture was washed by deionized water, and the organic phase was dried by anhydrous magnesium sulphate before removing the solvent with a rotary evaporator. The obtained powder was purified by silica gel column chromatography (toluene : hexane = 1 : 1) to afford a white solid (21.4 g, yield: 50%). ^{1}H NMR (300 MHz, $CDCl_3$) δ (ppm): 7.42–7.55 (m, 6H), 7.07–7.15 (m, 6H), 5.72 (s, 1H), 2.57–2.62 (t, J = 6.8 Hz, 2H), 1.60–1.65 (m, 2H), 1.30–1.33 (m, 10H), 0.89–0.92 (m, 3H). ^{13}C NMR (75 MHz, $CDCl_3$) δ (ppm): 143.9, 140.1, 140.0, 136.8, 132.0, 131.6, 129.5, 128.1, 127.9, 120.7, 119.3, 116.9, 35.5, 32.1, 31.9, 29.7, 29.6, 29.5, 22.9, 14.4.

Synthesis of COTPA [5], COTPA [6] and COTPA [7]

To a solution of monomer **1** (12.86 g, 29.47 mmol), potassium *t*-butoxide (3.31 g, 29.47 mmol), and palladium(II) acetate (0.29 g, 1.29 mmol) in dry toluene (920 mL) was added tri(*t*-butyl) phosphine (0.16 mL) under nitrogen atmosphere. The mixture was stirred at reflux for 24 h. After completion of the reaction, the solution was poured into methanol, and the mixture of polymers and oligomers was filtered as a precipitate. The collected mixture was subjected to Soxhlet extraction with butanone to separate the oligomers from the polymers. The resulted butanone solution was concentrated with a rotary evaporator and the crude product was purified by silica gel column chromatography with toluene/hexane (2/3 in volume ratio) to remove the linear oligomers. The mixture of cyclic oligomers was separated by preparative gel permeation chromatography. The yield of **COTPA [5]**, **COTPA [6]** and **COTPA [7]** was 3.1%, 3.6%, and 2.7%, respectively.

COTPA [5]. ^{1}H NMR (500 MHz, CD_2Cl_2) δ (ppm): 7.43–7.45 (d, J = 10.0 Hz, 4H), 7.04–7.10 (m, 8H), 2.56–2.59 (t, J = 7.8 Hz, 2H), 1.60–1.63 (m, 2H), 1.29–1.35 (m, 10H), 0.88–0.91 (t, J = 7.0 Hz, 3H); ^{13}C NMR (126 MHz, CD_2Cl_2) δ (ppm): 147.8, 145.2, 138.1, 135.4, 129.7, 127.8, 125.4, 123.7, 35.9, 32.5, 32.2, 30.1, 30.0, 29.9, 23.3, 14.4; MALDI-TOF-MS: m/z = 1777.473 ([M + H]$^+$, 100%), calcd for $C_{130}H_{145}N_5$ 1778.161; UV-vis (in toluene): λ_{max} = 350 nm; m.p. > 300 °C.

COTPA [6]. ^{1}H NMR (500 MHz, CD_2Cl_2) δ (ppm): 7.45–7.47 (d, J = 8.5 Hz, 4H), 7.05–7.13 (m, 8H), 2.57–2.60 (t, J = 7.5 Hz, 2H), 1.61–1.64 (m, 2H), 1.27–1.34 (m, 10H), 0.88–0.91 (t, J = 6.75 Hz, 3H); ^{13}C NMR (126 MHz, CD_2Cl_2) δ (ppm): 147.4, 145.4, 138.8, 135.0, 129.8, 127.7, 125.3, 124.5, 35.9, 32.5, 32.2, 30.1, 30.0, 29.9, 23.3, 14.5; MALDI-TOF-MS: m/z = 2133.201 ([M + H]$^+$, 100%), calcd for $C_{156}H_{174}N_6$ 2133.391; UV-vis (in toluene): λ_{max} = 349 nm; m.p. > 300 °C.

COTPA [7]. ^{1}H NMR (500 MHz, CD_2Cl_2) δ (ppm): 7.44–7.46 (d, J = 9.0 Hz, 4H), 7.05–7.13 (m, 8H), 2.57–2.60 (t, J = 7.8 Hz, 2H), 1.59–1.65 (m, 2H), 1.29–1.33 (m, 10H), 0.88–0.91 (t, J = 7.0 Hz, 3H); ^{13}C NMR (126 MHz, CD_2Cl_2) δ (ppm): 147.3, 145.6, 139.0, 135.0, 129.9, 127.7, 125.6, 124.2, 35.9, 32.5, 32.2, 30.1, 30.0, 29.9, 23.3, 14.5; MALDI-TOF-MS: m/z = 2489.883 ([M + H]$^+$, 100%), calcd for $C_{182}H_{203}N_7$ 2489.624; UV-vis (in toluene): λ_{max} = 347 nm; m.p. > 300 °C.

Synthesis of 4-[(2-ethylhexyl)oxy]nitrobenzene

[49]*p*-Nitrophenol (88.79 g, 638.6 mmol), 1-bromo-2-ethylhexane (112.00 g, 583.2 mmol), potassium carbonate (88.07 g, 638.6 mmol) and *N*,*N*-dimethylformamide (280 mL) was added into a 500 mL flask. The reactant was stirred at 80 °C for 48 h under nitrogen atmosphere. The reaction mixture was separated by NaOH (aq) solution and toluene, the organic phase was dried over anhydrous magnesium sulphate before removing the solvent with a rotary evaporator. A faint yellow liquid (113.9 g, yield: 78%) was obtained. ^{1}H NMR (300 MHz, $CDCl_3$) δ (ppm): 8.18–8.21 (d, J = 9.3 Hz, 2H), 6.94–6.97 (d, J = 9.3 Hz, 2H), 3.93–3.95 (d, J = 5.4 Hz, 2H), 1.70–1.82 (m, 1H), 1.29–1.57 (m, 8H), 0.89–0.96 (m, 6H).

Synthesis of 4-[(2-ethylhexyl)oxy]aniline

[50]4-[(2-Ethylhexyl)oxy]nitrobenzene (54.76 g, 218.0 mmol), palladium carbon (5.50 g), ethanol (50 mL) was added into a 500 mL flask. The reactant was stirred at room temperature for 72 h. The reaction mixture is filtered through Celite, and a black solid (37.1 g, yield: 77%) was obtained after removing the solvent. ^{1}H NMR (300 MHz, $CDCl_3$) δ (ppm): 6.61–6.76 (m, 4H), 3.75–3.77 (d, J = 6.0 Hz, 2H), 3.40 (s, 2H), 1.62–1.72 (m, 1H), 1.24–1.52 (m, 8H), 0.87–0.93 (m, 6H).

Synthesis of monomer 2

[50]4-[(2-Ethylhexyl)oxy]aniline (91.06 g, 411.4 mmol), 4,4′-dibromobiphenyl (42.78 g, 137.1 mmol), sodium *t*-butoxide (52.76 g, 549.2 mmol), dichloro[1,1′-bis(diphenylphosphino)ferrocene] palladium(II) (2.01 g, 2.46 mmol) and toluene (400 mL) was added in a 1000 mL flask under nitrogen atmosphere. The reactant was stirred and refluxed for 24 h. After completion of the reaction, the mixture was washed by saturated NaCl solution, and the organic phase was dried over anhydrous magnesium sulphate before removing the solvent by using a rotary evaporator. The obtained residue was recrystallized by hexane

to afford a white solid (38.8 g, yield: 48%). ^{1}H NMR (300 MHz, $CDCl_3$) δ (ppm): 7.39–7.42 (d, J = 8.4 Hz, 4H), 7.06–7.09 (d, J = 8.7 Hz, 4H), 6.93–6.96 (d, J = 8.4 Hz, 4H), 6.85–6.88 (d, J = 8.7 Hz, 4H), 5.52 (s, 2H), 3.81–3.83 (d, J = 5.7 Hz, 4H), 1.66–1.76 (m, 2H), 1.32–1.56 (m, 16H), 0.89–0.96 (m, 12H).

Synthesis of CETPA [6]

To a solution of monomer **2** (4.00 g, 6.75 mmol), 4,4′-dibromobiphenyl (2.11 g, 6.76 mmol), potassium *t*-butoxide (2.19 g, 19.5 mmol), and palladium(II) acetate (79.9 mg, 0.36 mmol) in dry xylene (700 mL) was added tri(*t*-butyl)phosphine (0.34 mL, 1.36 mmol) under nitrogen atmosphere. The mixture was reflux for 72 h. After completion of the reaction, the mixture was filtered through active clay, and the concentrated solution was re-precipitated by the addition of acetone. After filtration, the green solid was re-dissolved in hot *c*-hexane and then filtered to remove the insoluble impurity. A yellow solid was obtained after the filtrate was cooling down to room temperature. The yellow solid was re-crystallization in *o*-xylene, and the target product was obtained after filtration and dried in vacuum oven (256 mg, yield: 5.1%). ^{1}H NMR (500 MHz, CD_2Cl_2) δ (ppm): 7.41–7.42 (d, J = 8.5 Hz, 4H), 6.85–7.04 (m, 8H), 3.84–3.85 (d, J = 4.5 Hz, 2H), 1.72–1.74 (m, 1H), 1.35–1.54 (m, 8H), 0.92–0.96 (m, 6H); ^{13}C NMR (126 MHz, CD_2Cl_2) δ (ppm): 156.9, 147.6, 140.6, 134.6, 127.8, 127.6, 123.7, 115.9, 71.3, 40.1, 31.1, 29.7, 24.4, 23.7, 14.4, 11.5; MALDI-TOF-MS: m/z = 2227.867 ($[M + H]^+$, 100%), calcd for $C_{156}H_{174}N_6O_6$ 2229.360; UV-vis (in toluene): λ_{max} = 349 nm; m.p. > 300 °C.

Measurement of binding constants (K_a)

The host (**H**) solutions were prepared by dissolving CTPAs in toluene at a concentration of 5×10^{-6} M, and the guest (**G**) solutions were prepared by dissolving fullerenes in **H** solutions at a concentration of 2.5×10^{-4} M. Fluorescence spectra was determined when every 0.01 mL of **G** solution was added in 2 mL of **H** solution. K_a was calculated by the modified Benesi–Hildebrand equation $I_0/(I - I_0) = \{a/(b - a)\}\{(1/K_a)[\text{Guest}]_0^{-1} + 1\}$. In equation, a and b are constants while I and I_0 are the emission intensity at about 420 nm in 298 K with concentration of $[\text{Guest}]_0$ and 0, respectively.

Space-charge-limited current measurements

The device was fabricated by spin coating with indium tin oxide (ITO, 10 Ω sq^{-1})/poly(3,4-ethylenedioxythiophene):poly(styrenesulfonate) (PEDOT:PSS, 30 nm)/active layer (100–120 nm)/Au (40 nm) configuration. PEDOT:PSS with 30 nm of thickness was spin-coated on the substrate at 2500 rpm for 45 s from the dispersion in water filtered by 0.2 μm of membrane filter, followed by annealed at 120 C for 1 h under air. Then, solutions of **COTPA [5]** or **COTPA [5]** blended with C_{60} in chlorobenzene was spin-coated at 1000 rpm for 60 s on top of the PEDOT:PSS layer. The electrode (gold) was thermally deposited under vacuum. Space-charge-limited current measurements were carried out using Keithley 2400 (I–V) source meter.

Conflicts of interest

There are no conflicts to declare.

Acknowledgements

We thank the National Natural Science Foundation of China (22071040), the Science & Technology Innovation Program of Zhejiang Province (2018R52051) and Institute of Global Innovation Research in TUAT for financial support.

Notes and references

1 Y. Shirota and H. Kageyama, *Chem. Rev.*, 2007, **107**, 953–1010.
2 P. Agarwala and D. Kabra, *J. Mater. Chem. A*, 2017, **5**, 1348–1373.
3 P. Blanchard, C. Malacrida, C. Cabanetos, J. Roncali and S. Ludwigs, *Polym. Int.*, 2019, **68**, 589–606.
4 U. Bach, D. Lupo, P. Comte, J. E. Moser, F. Weissortel, J. Salbeck, H. Spreitzer and M. Gratzel, *Nature*, 1998, **395**, 583–585.
5 M. M. Lee, J. Teuscher, T. Miyasaka, T. N. Murakami and H. J. Snaith, *Science*, 2012, **338**, 643–647.
6 Y. Wang, Z. Yuan, G. Shi, Y. Li, Q. Li, F. Hui, B. Sun, Z. Jiang and L. Liao, *Adv. Funct. Mater.*, 2016, **26**, 1375–1381.
7 Z. Hawash, L. K. Ono and Y. Qi, *Adv. Mater. Interfaces*, 2018, **5**, 1700623.
8 J. Ohshita, K. Kondo, Y. Adachi, M. Song and S. Jin, *J. Mater. Chem. C*, 2021, **9**, 2001–2007.
9 Y. Song, C. Di, W. Xu, Y. Liu, D. Zhang and D. Zhu, *J. Mater. Chem.*, 2007, **17**, 4483–4491.
10 Z. Fang, M. Samoc, R. D. Webster, A. Samoc and Y. Lai, *Tetrahedron Lett.*, 2012, **53**, 4885–4888.
11 Q. Kong, H. Qian, Y. Zhou, J. Li and H. Xiao, *Mater. Chem. Phys.*, 2012, **135**, 1048–1056.
12 J. Y. Xue, T. Izumi, A. Yoshii, K. Ikemoto, T. Koretsune, R. Akashi, R. Arita, H. Taka, S. Sato and H. Isobe, *Chem. Sci.*, 2016, **7**, 896–904.
13 M. Ball, B. Zhang, Y. Zhong, B. Fowler, S. Xiao, F. Ng, M. Steigerwald and C. Nuckolls, *Acc. Chem. Res.*, 2019, **52**, 1068–1078.
14 S. Izumi, H. F. Higginbotham, A. Nyga, P. Stachelek, N. Tohnai, P. Silva, P. Data, Y. Takeda and S. Minakata, *J. Am. Chem. Soc.*, 2020, **142**, 1482–1491.
15 J. Xie, X. Li, S. Wang, A. Li, L. Jiang and K. Zhu, *Nat. Commun.*, 2020, **11**, 3348.
16 Y. Liu, H. Wang, L. Shangguan, P. Liu, B. Shi, X. Hong and F. Huang, *J. Am. Chem. Soc.*, 2021, **143**, 3081–3085.
17 Y. Liu, H. Wang, P. Liu, H. Zhu, B. Shi, X. Hong and F. Huang, *Angew. Chem., Int. Ed.*, 2021, **60**, 5766–5770.
18 F. Picini, S. Schneider, O. Gavat, A. V. Jentzsch, J. Tan, M. Maaloum, J. Strub, S. Tokunaga, J. Lehn, E. Moulin and N. Giuseppone, *J. Am. Chem. Soc.*, 2021, **143**, 6498–6504.
19 M. Iyoda, J. Yamakawa and M. J. Rahman, *Angew. Chem., Int. Ed.*, 2011, **50**, 10522–10553.

20 S. Wang, Y. Shen, B. Zhu, J. Wu and S. Li, *Chem. Commun.*, 2016, **52**, 10205–10216.
21 P. S. Bols and H. L. Anderson, *Acc. Chem. Res.*, 2018, **51**, 2083–2092.
22 M. Hermann, D. Wassy and B. Esser, *Angew. Chem., Int. Ed.*, 2021, **60**, 15743–15766.
23 B. Lu, Z. Zhang, J. Wang, G. Cai, J. Wang, X. Yuan, Y. Ding, Y. Wang and Y. Yao, *Mater. Chem. Front.*, 2021, **5**, 5549–5572.
24 H. W. Kroto, J. R. Heath, S. C. O'Brien, R. F. Curl and R. E. Smalley, *Nature*, 1985, **318**, 162–163.
25 A. Kost, L. Tutt, M. B. Klein, T. K. Dougherty and W. E. Elias, *Opt. Lett.*, 1993, **18**, 334–336.
26 R. Charvet, Y. Yamamoto, T. Sasaki, J. Kim, K. Kato, M. Takata, A. Saeki, S. Seki and T. Aida, *J. Am. Chem. Soc.*, 2012, **134**, 2524–2527.
27 S. H. Friedman, D. L. DeCamp, R. P. Sijbesma, G. Srdanov, F. Wudl and G. L. Kenyon, *J. Am. Chem. Soc.*, 1993, **115**, 6506–6509.
28 R. Bakry, R. M. Vallant, M. Najam-ul-Haq, M. Rainer, Z. Szabo, C. W. Huck and G. K. Bonn, *Int. J. Nanomed.*, 2007, **2**, 639–649.
29 P. Innocenzi and L. Stagi, *Chem. Sci.*, 2020, **11**, 6606–6622.
30 N. S. Sariciftci, L. Smilowitz, A. J. Heeger and F. Wudl, *Science*, 1992, **258**, 1474–1476.
31 I. Hong, M. Lee, Y. Koo, H. Jeong, T. Kim and O. Song, *Appl. Phys. Lett.*, 2005, **87**, 063502.
32 J. Y. Lee, *Appl. Phys. Lett.*, 2006, **88**, 073512.
33 Y. J. He and Y. F. Li, *Phys. Chem. Chem. Phys.*, 2011, **13**, 1970–1983.
34 T. Iwamoto, Y. Watanabe, T. Sadahiro, T. Haino and S. Yamago, *Angew. Chem., Int. Ed.*, 2011, **50**, 8342–8344.
35 H. Shimizu, J. D. C. Gonzalez, M. Hasegawa, T. Nishinaga, T. Haque, M. Takase, H. Otani, J. P. Rabe and M. Iyoda, *J. Am. Chem. Soc.*, 2015, **137**, 3877–3885.
36 E. Q. Procopio, T. Benincori, G. Appoloni, P. R. Mussini, S. Arnaboldi, C. Carbonera, R. Cirilli, A. Cominetti, L. Longo, R. Martinazzo, M. Panigati and R. Po, *New J. Chem.*, 2017, **41**, 10009–10019.
37 H. Shimizu, K. H. Park, H. Otani, S. Aoyagi, T. Nishinaga, Y. Aso, D. Kim and M. Iyoda, *Chem.–Eur. J.*, 2018, **24**, 3793–3801.
38 B. Zhu, H. Chen, W. Lin, Y. Ye, J. Wu and S. Li, *J. Am. Chem. Soc.*, 2014, **136**, 15126–15129.
39 E. R. Darzi, E. S. Hirst, C. D. Weber, L. N. Zakharov, M. C. Lonergan and R. Jasti, *ACS Cent. Sci.*, 2015, **1**, 335–342.
40 J. C. Barnes, E. J. Dale, A. Prokofjevs, A. Narayanan, I. C. Gibbs-Hall, M. Jurícek, C. L. Stern, A. A. Sarjeant, Y. Y. Botros, S. I. Stupp and J. F. Stoddart, *J. Am. Chem. Soc.*, 2015, **137**, 2392–2399.
41 S. Wang, W. Lin, X. Wang, T. Cen, H. Xie, J. Huang, B. Zhu, Z. Zhang, A. Song, J. Hao, J. Wu and S. Li, *Nat. Commun.*, 2019, **10**, 1399.
42 S. Zhang, Z. Liu, W. Fu, F. Liu, C. Wang, C. Sheng, Y. Wang, K. Deng, Q. Zeng, L. Shu, J. Wan, H. Chen and T. P. Russell, *ACS Nano*, 2017, **11**, 11701–11713.
43 J. Simokaitiene, M. Cekaviciute, D. Volyniuk, G. Sini, C. Voz, J. Puigdollers, A. Bucinskas and J. V. Grazulevicius, *Org. Electron.*, 2019, **73**, 137–145.
44 K. Tsuchiya, H. Miyaishi and K. Ogino, *Chem. Lett.*, 2011, **40**, 931–933.
45 K. Kim, R. Ohata, S. Kanehashi, K. Tsuchiya and K. Ogino, *Chem. Lett.*, 2017, **46**, 1145–1147.
46 A. V. Nikolaev, T. S. Dennis, K. Prassides and A. K. Soper, *Chem. Phys. Lett.*, 1994, **223**, 143–148.
47 D. Canevet, M. Gallego, H. Isla, A. d. Juan, E. M. Perez and N. Martín, *J. Am. Chem. Soc.*, 2011, **133**, 3184–3190.
48 M. Frisch, G. Trucks, H. Schlegel, G. Scuseria, M. Robb, J. Cheeseman, G. Scalmani, V. Barone, G. Petersson and H. Nakatsuji, Gaussian Inc., Wallingford CT, 2016.
49 S. Ji, M. Shigeta, Y. Niko, J. Watanabe and G. Konishi, *Tetrahedron Lett.*, 2013, **54**, 7103–7106.
50 D. H. Oh, Q. Zhao, S. Kim, H. Park, Y. Kim, Y. Park, J. Kim and S. Kwon, *Macromol. Res.*, 2011, **19**, 629–634.